Color tuning of face-selective neurons in cells in macaque inferior temporal cortex

Marianne Duyck, Tessa J. Gruen, Lawrence Y. Tello, Serena Eastman, Joshua Fuller-Deets, Bevil R. Conway

How are face-specific color signals encoded by the brain? We addressed this question by measuring color responses of face-selective cells in alert macaque monkey, using fMRI-guided microelectrode recording of the middle and anterior face patches. Many face-selective neurons showed broad color tuning when assessed using images that preserved the luminance contrast relationships of the original face photographs. A Fourier analysis of the color-tuning responses uncovered two components. The first harmonic showed a bias towards the L>M pole of the L-M cardinal axis of cone-opponent color space (appearing reddish), which suggests that face cells encode a prior about the color component of faces that is important for social signaling (blood perfusion). The second harmonic showed a bias for colors that modulate the S-cone cardinal axis, which may relate to the computation of animacy by IT cells. Taken together, these results uncover a putative physiological basis for the role of color in face perception and show that chromatic signatures corresponding to the cardinal chromatic mechanisms are evident not only in subcortical circuits, as previously known, but also far along the visual-processing hierarchy, within inferior temporal cortex.

Significance: *It is not known how the brain processes combined color and face information. The present results fill this gap in knowledge by uncovering the color tuning properties of face-selective neurons. The results further our understanding of the neural mechanisms that make color an informative cue for social communication.*

Color is neither necessary nor sufficient for face recognition: People can identify faces in black and white photographs and are impaired at recognizing faces in pictures that have color contrast but lack luminance contrast (Sinha et al., 2006). These observations suggest that the neural machinery for face recognition is color blind (Webster and MacLeod, 2011), an idea that is supported by adaptation experiments, which fail to show interactions between face and color processing (Yamashita et al., 2005). Consequently, most behavioral and neuronal studies of face perception have used achromatic stimuli (Kanwisher et al., 1997; Ohayon et al., 2012).

Although color is not essential for determining face identity, face color nonetheless relays important social information about health, emotion, sex, and social status (Setchell and Wickings, 2005; Changizi et al., 2006; Waitt et al., 2006; Gerald et al., 2009; Leopold and Rhodes, 2010; Lefevre et al., 2013; Petersdorf et al., 2017). Face color may influence how facial emotions are recognized (Nakajima et al., 2017); there is a slight color difference between the average male and female face, which can facilitate gender discrimination when shape cues are degraded (Nestor and Tarr, 2008; Webster and MacLeod, 2011); and memory strongly modulates the perception of face color (Hasantash et al., 2019). The dynamic social chromatic signals appear to be relayed by variation along the red-green (L-M) axis of color space (Hasantash et al., 2019), which predominantly reflects oxygenation of hemoglobin and skin perfusion, and to a lesser extent ingested carotenoids from foods.

How does the brain encode face-specific color information? One possibility is that face-selective cells carry color information. This possibility is suggested by two observations using fMRI: there is broad color tuning of the ventral visual pathway, encompassing the face-processing network, which shows a bias for warm (L>M) colors (Rosenthal et al., 2018); and face-selective cortex can be modulated by changing stimulus color (Nakajima et al., 2014). Cells in macaque temporal cortex can show both complex shape selectivity and color sensitivity (Komatsu and Ideura, 1993; Edwards et al., 2003), but color tuning of face-selective neurons has not been systematically addressed.

Here we ask whether face-selective neurons within the ventral visual pathway are sensitive to color. And if so, are they color tuned? We measured responses in the middle and anterior face patches of macaque monkeys using fMRI-guided recording. In the first set of experiments, the stimuli were face photographs comprised of both luminance contrast and color. In the second set of experiments, the stimuli were face photographs that were manipulated to remove luminance contrast so that the face-shape information was determined only by equiluminant colors. Most face cells were not very responsive to equiluminant stimuli, consistent with prior work showing the importance of luminance contrast in face-cell responses (Ohayon et al., 2012). But many face-selective cells were nonetheless color tuned when using stimuli defined by luminance contrast and color. The tuning of these neurons was biased for colors eliciting higher L>M activity, consistent with the idea that these cells encode a prior about the behaviorally relevant component of face color.

Results

Functional magnetic resonance imaging was used to identify regions of inferior temporal cortex that were more responsive to faces than to bodies and fruits, a standard contrast used to identify face patches (Tsao et al., 2006; Lafer-Sousa and Conway, 2013). We targeted microelectrodes to the ML face patch in two monkeys (M1 and M2) and the AL face patch in three monkeys (M1, M2 and M3; **Figure 1A**). To screen for face-selective neurons, we measured the responses of each cell to a battery of grayscale images of 14 categories (**Figure 1B**). Face-selective neurons, such as the two examples in Figure 1B, were defined as those that showed at least a twofold greater response to faces than bodies and fruits. This selection criterion yielded 102 single units in ML and 71 single units in AL. Face-selective cells in AL had a higher face selectivity index than cells in ML (**Figure 1C**; Mdn_{ML} = 0.60, Mdn_{AL} = 0.92, Mann-Whitney-Wilcoxon rank-sum test U=1842, p<0.001); cells in AL and ML had similar firing rates (Mdn_{ML} = 6.38, Mdn_{AL} = 6.28, U=3671, p>0.88).

We measured responses to color for those cells that showed a face-selectivity index (FSI) greater than or equal to 1/3. Color responses were obtained using monochromatic versions of photographs of faces, bodies, and fruits (**Figure 2A**); the colored stimuli evenly sampled CIELUV color space (**Figure 2B**, top panel). We chose to define the stimuli in CIELUV color space because this space captures the representation of color within the V4 Complex (Bohon et al., 2016), which provides input into inferior temporal cortex (Kravitz et al., 2012). The chromaticity of the stimuli can be transformed into cone-opponent space, which reflects the cone-opponent cardinal mechanisms evident in the lateral geniculate nucleus (Derrington et al., 1984; Sun et al., 2006) (**Figure 2B**, bottom panel). To create a given image in a target color, we replaced each gray value of the original achromatic image with the target hue of the same luminance value. Thus the false-colored images maintained the luminance contrast of the original image.

Figure 3 shows the responses of a representative sample of six face-selective neurons to the colored images of faces, bodies, and fruit; cells 1-3 were recorded in face patch ML; cells 4-6 were recorded in face patch AL. The top panels show the average responses to images of faces, bodies, and fruits. As predicted given the screening criterion, responses were always substantially larger to faces than to the other stimulus categories, with face-selectivity indices ranging from 0.44 to ~1. For each cell we defined a time period for quantification of the responses (blue bar in **Figure 3A, 3B**). We used a single continuous time period for all cells whose duration was tailored to each cell. The response of cells showed complex temporal dynamics. For example, cell #4 showed two peaks (at 105 ms and 225 ms) and the intervening firing rate dipped back to baseline—in cells such as this one, the time period for quantification only included the initial peak. Using multiple time periods for some cells such as cell #4 did not change the main conclusions (data not shown). The median latencies and the duration of the response time periods across the population of cells are reported in **Table 1**. Cells in ML showed a shorter latency than cells in AL within each monkey. But the variability in latencies for cells in ML or AL across monkeys was greater than the difference in latency between ML and AL within any monkey.

The top panels in **Figure 3B** show post-stimulus-time-histograms (PSTHs) of the responses to the colored faces, averaging across the four different face categories we used (monkey and human faces, frontal faces and ¾-view faces; see Figure 1B). The orientation of the PSTH shows time on the y-axis and image color on the x-axis. The stimulus onset is at 0 seconds, and darker gray corresponds to higher firing rate. The responses of the neurons are delayed by a latency reflecting the time for visual signals to be processed by the retina and relayed through the visual-processing hierarchy to inferior temporal cortex. The cells in **Figure 3** were representative of the population: three of the cells were modulated by the color of the stimulus (cells #1, #3, #6), reflected in the average response over the response window (black trace below the PSTH; see methods for significance calculation). Among the population of face-selective neurons, ~25% were significantly modulated by color (23/102 cells in ML; 21/71 cells in AL). Cells #2, #4, and #5 were not modulated significantly by color. The red traces in Figure 3B show the best-fitting sine wave following Fourier analysis of the color responses, described below.

Note that the firing rates shown in the bottom panels of **Figure 3B** are averages over the response window and so are lower than the peak firing rates shown in **Figure 3A**. Although many cells were modulated by color, the variance in firing rate caused by changes in color was modest. For example, the firing rate in cell #3 varied between 18 and 22 spikes/second above background, which corresponds to +/- 10% of the average stimulus-driven response. Across the population, the variation in firing rate due to hue was +/-24% of the average stimulus-driven response. Most of the stimulus-driven response can likely be attributed to the luminance contrast of the images (see **Figure 9B**).

Figure 3C plots the cells' responses as a function of color angle; the norm of the vector sum is shown as the bolded black line, and varies between 0 and 1 (0=equal net firing rate for all hues, i.e. no color tuning; values for each cell are shown in black text). To further quantify the results, we determined the best-fitting sine wave of the color-tuning response for each cell (red lines, **Figure 3B**). Most cells (71/173) were best fit by the first harmonic (a single cycle), which shows that these cells have a single preferred color (see cell #3, #6, **Figure 3**); but some cells were best fit by the second harmonic (21/173), indicative of a preference for a color axis in color space, rather than a single color direction (cell #1, **Figure 3**). The amplitude and phase angle of the best fitting harmonic is shown in red in **Figure 3C**. The color preferences assessed by the norm of the vector sum and the normalized amplitude of the first harmonic were highly correlated (Pearson $r=0.93$, $p<0.001$). Among the 44 cells showing significant color

modulation, the power of both the first and the second harmonic was higher than the noise level estimated as the power to the 8th harmonic (red lines, **Figure 4**); 37/44 cells showed highest power to the first harmonic; 5/44 showed highest power to the second harmonic; 1/44, to the third; and 1/44 to the fourth.

Figures 3 and 4 provide evidence that some face-selective cells were sensitive to color. Among the population, was there a consistent color preference? **Figure 5** shows the color responses of all the face-selective cells rank ordered by the significance of the color tuning, with the most significantly color-tuned cells at the top. Each row shows data from one cell. The gray level shows the normalized response to the given color (the sum of the values across colors for a given cell is 1). Many of the most significantly color tuned neurons in both ML and AL preferred warm colors, as evident by the dark regions on the upper left and right of the panels in Figure 5. But there were some exceptions. For example, cells represented by rows 6 and 7 in the ML panel and rows 1 and 2 in the AL panel of Figure 5 showed a preference for greenish colors.

Figure 6 quantifies the color responses of the population of single cells using Fourier analysis. The left panel of Figure 6A shows a polar histogram of the peak color direction for cells with maximum power to the first harmonic; significantly color-tuned cells are shown in dark gray. These results confirm the population bias towards the L>M pole of the L-M cardinal axis. This bias is also evident when analyzing the color direction of the best-fitting first harmonic for all cells in the population (including those that did not have maximum power in the first harmonic, **Figure 6B**, left panel). In contrast, cells with maximum power to the second harmonic showed a phase angle biased for the S-cone cardinal axis (**Figure 6A**, right panel). And this bias was also evident when analyzing the best fitting second harmonic for all cells in the population (including those that did not have maximum power in the second harmonic; **Figure 6B**, right panel).

How does color tuning relate to color selectivity? If color tuning reflects a computational objective of the circuit one might predict that within the population more color-selective cells will have more consistent color tuning. **Figure 7** quantifies the norm of the vector average (i.e. the peak color preference; y-axis), color selectivity (x-axis), significance of color tuning (symbol gray value), and number of stimulus repeats obtained (symbol size). The data points to the right of the plot converge on 0 degrees (the L>M pole of the L-M axis), consistent with the prediction. Significantly color tuned neurons, defined by the $p<0.05$ threshold had a mean preferred hue angle that did not differ from insignificantly color tuned neurons (Watson-Williams test, $F(1, 171)=0.07$, $p=0.80$) but had a significantly lower variance (**Figure 7**, marginal distribution, Wallraff test, $\chi^2=11.59$, $p<0.001$). This effect cannot be attributed to variance in the amount of data collected for different neurons. To prove this, we split the population into two groups, above and below the median number of trials collected per cell. The variance in the peak color tuning was the same for both groups (Wallraff test, $\chi^2=1.10$, $p=0.29$).

The face-selective neurons responded strongly to all the colored stimuli, even those of suboptimal color (see Figure 3), which we attribute to the luminance contrast of the stimuli (regardless of the color, the stimuli preserved the luminance contrast of the original images). We can directly dissect the role of color and luminance contrast on the cell responses by using equiluminant colored stimuli (**Figure 8A**). These stimuli were created by replacing the range of gray values in the original images with colors of a constant gray value but different saturation: higher luminance gray values were replaced with more saturated color. Responses to these equiluminant stimuli were substantially lower than responses to the

colored stimuli that preserved luminance contrast (**Figure 8B**; Mdn_{Iso} = 0.99, Mdn_{Main} = 7.64, Wilcoxon rank-sum test U=4643, p<0.001). These results show that pure color is not sufficient to strongly drive face-selective cells.

We previously measured the color responses across IT using fMRI (Lafer-Sousa and Conway, 2013; Rosenthal et al., 2018). To directly compare the results of the fMRI with the cell data, we quantified the neural responses within a 400 ms time window starting at the stimulus onset. This time window encompasses the 200 ms duration of the stimulus and the 200 ms inter-stimulus gray period. **Figure 9A** shows the average response for the population, in ML (solid line) and AL (dotted line). The plot shows significant differences among the responses to the colors (non-parametric Friedman test, χ^2= 210.69, p<0.001) and the responses in ML are highly correlated with those in AL (Pearson r=0.89, p<0.001). **Figure 9B** shows the average response across all face-selective cells to face images in each of the 16 colors. This plot underscores two main conclusions: first, responses to all colored images were strong, which we attribute to the fact that all the colored exemplars preserved the luminance contrast of the original achromatic images—the luminance contrast is a main determinant of face-selective responses (Ohayon et al., 2012); and second, among the colored stimuli, responses to the L>M stimuli (appearing pinkish) were higher than response to the M<L stimuli (appearing greenish). The color biases of the population of face-selective cells was strongly correlated with the color biases of the face patches measured with fMRI (**Figure 9C**, Pearson r=0.64 p=0.008).

Discussion

Here we document for the first time the color responses of face-selective neurons in macaque inferior temporal cortex. The results provide evidence that the population of face-selective neurons shows a bias for warm colors, consistent with the hypothesis that these cells encode a prior about the behaviorally relevant component of face color (Hasantash et al., 2019). The color bias was measured using images that preserve the normal luminance contrast relationships of face photographs. In a second series of experiments, we found that face-selective cells were not very responsive to pure color (equiluminant) images of faces. The results confirm prior results showing the importance of luminance contrast for face selectivity (Ohayon et al., 2012), and provide single-unit evidence supporting the fMRI observation that face patches respond more strongly to luminance contrast compared to equiluminant color (Lafer-Sousa and Conway, 2013).

How do the color-tuning results relate to the role of color in behavior? Optimal neural coding requires that there be a good match between neural tuning and environmental statistics (Simoncelli and Olshausen, 2001). We might therefore expect an agreement between neural tuning and the statistics of those parts of the environment that are behaviorally relevant (Wei and Stocker, 2015). Face color is important for behavior in trichromatic primates, providing a cue to sex, dominance, health, and emotion (Waitt et al., 2003; Setchell and Wickings, 2005; Dubuc et al., 2009; Stephen et al., 2009; Hiramatsu et al., 2017; Conway, 2018). Moreover, faces occupy a distinct gamut in color space (Crichton et al., 2012; Chauhan et al., 2015), in which the dynamic color component is determined predominantly by hemoglobin oxygenation (this is true for people regardless of race, as well as in non-human primates that have lost some facial hair such as macaque monkeys). These observations predict that if face-selective cells participate in color computations, the cells would be most responsive for colors that are most relevant in social signaling. Because warm coloring (L>M cone activity) is associated with social

signaling, we predicted that if face cells show a color bias, the population would be biased for warm colors. The neurophysiological results confirm this prediction. About 25% of face-selective neurons were significantly color tuned. Most of these cells were best described as having a single peak in the color-tuning function—with maximum power to the first harmonic in Fourier analysis of the color-tuning function—and the peaks across the population of cells were biased towards warm (L>M) colors.

That face-selective neurons are sensitive to color may be somewhat surprising in the context of behavioral work showing that color is neither necessary nor sufficient for face recognition under most circumstances (Yip and Sinha, 2002)—luminance-contrast is sufficient under almost all normal viewing conditions (Kemp et al., 1996)—and the lack of evidence in adaptation paradigms of interactions between face processing and color processing (Yamashita et al., 2005). But other behavioral work predicts that face cells carry chromatic signals, and specifically that the color bias in the population should reflect the likely color of the behaviorally relevant component of faces (Hasantash et al., 2019). Indeed, the behavioral results reported by Hasantash et al. prompted the present neurophysiological study. Hasantash et al. showed that under low-pressure sodium (LPS) illumination—a condition that impairs retinal mechanisms of color—memory has a profound impact on color appearance only for faces. Curiously under LPS light faces appear green, not their normal warm coloring. Similar paradoxical phenomena, in which a noisy sensory signal gives rise to a perception that is away from the prior, not towards it, have been observed in other domains, such as orientation, biological motion, and size/weight (Campbell and Maffei, 1971; Brayanov and Smith, 2010; Sweeny et al., 2012). The puzzle of these phenomena can be explained by a Bayesian observer model in which image statistics influence both encoding and decoding of sense signals (Wei and Stocker, 2015). Wei and Stoker's results imply that any empirical observations of seemingly anti-Bayesian phenomena are evidence of neural mechanisms that encode the relevant prior. Thus the observation that faces seen under LPS light appear green predicts that face-coding cells should be biased to reddish colors (complementary to green), corresponding to a prior about the behaviorally relevant component of skin color.

Is the warm color bias unique to face-selective cells? Inferior temporal cortex is implicated broadly in object vision, not just face recognition. Rosenthal et al. showed that the statistics of object colors are not arbitrary (Rosenthal et al., 2018): whether a pixel is part of an object can be estimated by the extent to which the pixel aligns with the L>M pole of the L-M axis in cone-opponent color space. Thus warm coloring is a distinguishing property of objects generally, not just faces, suggesting that non-face-selective IT cells may also be biased for warm colors. This hypothesis is supported by the functional organization of color tuning assessed with fMRI, which shows a broad band of tissue extending along the anterior-posterior extent of IT encompassing tissue inside and outside face patches (Conway, 2018; Rosenthal et al., 2018). In the present work, micro-electrode recordings occasionally glanced the margin of the face patches. The non-face-selective cells we encountered also showed a weak bias for warm colors (**Figure 10**). These results suggest that a warm bias is a consistent feature of IT cells. The warm bias we report is also consistent with the colors of optimal stimuli obtained in neural-response-guided machine learning experiments of IT cells (Ponce et al., 2019).

Although most cells had a single peak in the color-tuning function, some face-selective neurons were best fit by two peaks, with maximum power to the second harmonic in the Fourier analysis (**see example cell #1, Figure 3**). The color selectivity of this subset of neurons, assessed as the phase angle of the second harmonic, was aligned with the S-cone axis in color space (**Figure 6**). Is the tuning to the second harmonic meaningful? One might be concerned that these responses reflect a luminance

artifact: the estimate of equiluminance may not be accurate especially for colors that modulate S cones, despite appropriate corrections (Vos, 1978). We do not think these responses can be attributed to luminance artifacts because the stimuli preserved the luminance contrast of the original images (the blackest black and whitest white in the colored versions of each image were the same as in the original image). Any luminance artifact would be masked by the luminance contrast of the original image.

The response bias to colors along the S axis was surprising, but the color statistics of objects might provide an explanation. In addition to the observation that objects tend to be warm, Rosenthal et al. uncovered another property of the color statistics of objects: animacy can be predicted based only on the extent to which the color of the object modulates S cones. Thus the tuning to the second harmonic may enable the computation of animacy by IT cells. Regardless of the explanation, we think the results provide the first measurements of color tuning biases within extrastriate cortex that reflect the cardinal mechanisms: the first harmonic is tuned along the L-M cardinal axis and the second harmonic is tuned along the S cardinal axis. The cardinal mechanisms correspond to the color tuning of the cone-opponent cells that represent the first post-receptoral stage of color encoding and are reflected in the anatomy and physiology of the lateral geniculate nucleus (Derrington et al., 1984; Martin et al., 2001; Sun et al., 2006; Roy et al., 2009). The cardinal mechanisms are evident in behavioral work that is thought to isolate these subcortical contributions to color vision (Krauskopf et al., 1982; Eskew, 2009). The observation that cortical cells reflect the cardinal mechanisms is surprising because the distinct chromatic signatures associated with the cardinal mechanisms diffuse near the input layers to primary visual cortex (Tailby et al., 2008). The present results show that chromatic signatures corresponding to the cardinal mechanisms reemerge in extrastriate cortical circuits far along the putative visual-processing hierarchy, and they raise the possibility that the behavioral results reflecting the cardinal mechanisms may depend upon cortical, not subcortical, circuits.

Functional MRI response patterns in both macaque monkeys and humans show a multi-stage organizational scheme governed by a repeated eccentricity template, in which color-biased tissue is sandwiched between face-selective tissue (foveal biased) and place-selective tissue (peripheral biased) in parallel streams along the length of the ventral visual pathway (Lafer-Sousa and Conway, 2013; Lafer-Sousa et al., 2016; Conway, 2018). This organization might be incorrectly interpreted to imply that the only portions of IT that use color information are the color-biased regions. The results here support the hypothesis that color contributes to operations in most, if not all, of the parallel networks through IT, even those networks that are not explicitly color biased. A hypothesis we favor is that color-biased regions enable the decoding of surface hue in service of object recognition (Komatsu, 1998; Zaidi et al., 2014; Bohon et al., 2016; Conway, 2018), while color signals in other parts of visual cortex may facilitate object recognition by encoding relevant priors about lighting conditions (Lafer-Sousa et al., 2012) and object colors.

Methods

Subjects

Three male rhesus macaques (*Macaca mulatta*), weighing 8-10 kgs, were implanted with an MRI-compatible plastic (Delrin) chamber and headpost. Surgical implantation protocol has been described previously (Lafer-Sousa and Conway, 2013). Designation of the subjects are M1 (monkey 1), M2 (monkey 2), and M3 (monkey 3). Monkeys 1 and 3 (M1, M3) had chambers over the right hemisphere; Monkey 2 (M2) had a chamber on the left hemisphere. All procedures were approved by the Animal

Care and Use Committee of the National Eye Institute and complied with the regulations of the National Institutes of Health.

Functional Imaging targeting of Face Patches

The fMRI procedures we use for localizing face patches have been described (Lafer-Sousa and Conway, 2013; Rosenthal et al., 2018). Two of the animals (M1, M2) are the same as the animals used in Lafer-Sousa and Conway (2013); the face-patch data and color-tuning data are the same as in the earlier reports. Here, we present an analysis of the fMRI color-tuning data restricted to the face patches of inferior temporal cortex. All monkeys were scanned at the Massachusetts General Hospital Martinos Imaging Center in a Siemens 3T Tim Trio scanner. Magnetic resonance images were acquired with a custom-built four-channel magnetic resonance coil system with AC88 gradient insert, which increases the signal-to-noise ratio by allowing very short echo times, providing 1-mm3 spatial resolution and good coverage of the temporal lobe. We used standard echo planar imaging (repetition time = 2 s, 96 × 96 × 50 matrix, 1 mm^3 voxels; echo time = 13 ms). Monkeys were seated in a sphinx position in a custom-made chair placed inside the bore of the scanner, and they received a juice reward for maintaining fixation on a spot presented at the center of the screen at the end of the bore. An infrared eye tracker (ISCAN) was used to monitor eye movements, and animals were only rewarded by juice for maintaining their gaze within ~1 degree of the central fixation target. Magnetic resonance signal contrast was enhanced using a microparticular iron oxide agent – MION (Feraheme, 8–10 mg per kg of body weight, diluted in saline, AMAG Pharmaceuticals), injected intravenously into the femoral vein just before scanning.

Visual stimuli were displayed on a screen subtending 41 by 31 dva, at 49 cm in front of the animal using a JVC-DLA projector (1024 by 768 pixels). The subset of presented stimuli used here to localize face patches consisted in achromatic square photographs of faces and body parts presented centrally on a neutral gray screen (~25 $cd.m^{-2}$) and occupying 6 degrees. They were shown in 16 32-s blocks (16 repetition times per block, repetition time = 2 s, 2 images per repetition) presented in one run sequence. The images were matched in average luminance to the neutral gray, maintaining roughly constant average luminance (~25 $cd.m^{-2}$) throughout the stimulus sequence. For faces stimuli we used: 16 unique images front-facing of unfamiliar faces (8 human, 8 monkey), The bodies/body parts block comprised 32 unique images of monkey and human bodies (no heads/faces) and body parts. Face patches were localized by contrasting responses to faces versus responses to body parts. 18 runs were used to localize face patches in M1 and M2, and 16 runs were used to localize face patches in M3.

Physiological recordings

A plastic grid was fitted to the inside of the recording chamber to enable us to reproducibly target regions within the brain, following details reported previously (Conway et al., 2007). We used sharp epoxy-coated tungsten electrodes (FHC), propelled using a hydraulic manual advancer (Narishige). Voltage traces were digitized and saved with a Plexon MAP system (Plexon Inc., Dallas, TX). Spike waveforms were sorted offline with the Plexon Offline Sorter, and single units were defined on the basis of waveform and inter-spike interval.

Recordings were performed in a light-controlled room, with the animals seated in sphinx position. Animals were acclimatized to head restraint in order to minimize head movement during recordings. Animals maintained fixation on a spot on a monitor 57 cm away; the monitor was a CRT Barco subtending 40 by 30 dva, operating at 85 Hz and at a resolution of 1024 by 768 pixels. Eye position was

monitored throughout the experiments using and infrared eye-tracker (ISCAN). The monitor was color calibrated using a PR-655 SpectraScan Spectroradiometer (Photo Research Inc.); we achieved 14-bit resolution for each phosphor channel using Bits++ (Cambridge Research Systems).

Stimuli

Screening stimuli consisted in 10 grayscale exemplars of each of the 14 following categories: animals, buildings, human faces (front view), monkey faces (front view), human faces (3/4 view), monkey faces (3/4 view), fruits, furniture, monkey bodies (no face), human bodies (no face), places, technology objects, indoor places, natural scenes, vehicles. All stimuli were presented on a static luminance noise background of 7.5 by 7.5 degrees of visual angle.

Stimuli for the color-tuning experiments were exemplars of faces of unfamiliar humans and monkeys, front or ¾ view (16 exemplar of frontal view and 8 of ¾ view for each species), fruits known to the monkey (16 exemplars) and bodies/body parts (without head) of unfamiliar humans and monkeys (8 exemplars for each subcategory). For both sets of experiments using colored stimuli (main condition in which the colored stimuli preserved the luminance contrast of the original achromatic images, and the equiluminant condition) we defined 16 target hues equally spaced along the CIELuv color space. For the main condition (Figure 2), each pixel value of the original achromatic image was remapped to the most saturated target color of the same luminance value within the monitor gamut. For the equiluminant condition (Figure 8), each pixel value of the original image was remapped to a pixel on the equiluminant plane, of the same hue as the target but different saturation based on the pixel luminance (see Figure 8).

Note that one way of making false-colored images that has been used in some studies involves the digital equivalent of superimposing a color filter over a black and white picture. In these images, the white of the original image is replaced with a relatively saturated color. Although easy to generate, these false-colored images are luminance compressed compared to the original image: the black in the colored version remains the same luminance as the original, but the white is now a lower luminance than the white in the original. Moreover, it is possible that the estimation of luminance for a given color is inaccurate (see (Conway, 2009) for a discussion). Such inaccuracies would introduce variability in the luminance contrast among the different colored images generated using the color-filter method. The method used presently mitigates the possible impact of chromatic aberration and variability in macular pigmentation, and gives rise to images that are more naturalistic: the images not only retain the luminance contrast of the original images but also appear differently colored, rather than achromatic but viewed through a colored filter (see Golz and MacLeod, 2002).

Procedure

One experimental session started by targeting a microelectrode to a face patch, recording a single unit (selected online based on waveform), mapping the receptive field by hand, and choosing the visual-field location that gave the highest response to the screening stimuli. Then we recorded the neural activity while presenting the battery of screening stimuli. If a cell appeared face selective, we then recorded responses to the colored stimuli presented in random order.

Data Analysis

Response window

The response of each neuron was quantified within a response window defined using the average response to all stimuli, in 10 ms bins. The baseline firing rate of each cell was defined as the average response from 50 ms before stimulus onset to 10 ms after stimulus onset. The response window for each cell was determined as one continuous time period initiated when, within two consecutive time bins, the neural response increased above 2.5 standard deviations above the baseline firing rate and terminated either when the response dropped below 2.5 standard deviations of the baseline firing rate in two consecutive bins or after 200 ms following the start of the response window (the shorter of the two options was used). Cells were only included in the analysis if the response window was initiated between 50 ms and 250 ms after stimulus onset, and if the neural response was excitatory (i.e. cells showing suppressive responses to stimulus onset were not included).

Face selectivity

The present analysis focused on the color tuning of face-selective neurons. We targeted microelectrode recordings to face patches using fMRI to guide the microelectrode recordings. Face selectivity was assessed using the following index:

$$FSI = \frac{R_{face} - mean(R_{bodies}, R_{fruits})}{|R_{face}| + |mean(R_{bodies}, R_{fruits})|}$$

Where R is the average response to stimulus, computed as the difference between the firing rate during the response window and the firing rate during background. FSI values range from -1 to +1, with values above 0 indicating a higher response to faces compared to bodies and fruits. All analyses, with one exception, were restricted to neurons that showed an FSI =>1/3, corresponding to a response to faces at least twice than the response to other non-face stimuli. The exception was the last analysis (see Figure 9), in which we examined the relationship between hue preference and face selectivity. For that last analysis we included an additional 61 cells that were recorded by targeting the same face patches but had an FSI below 1/3.

Color Tuning

Significance of color modulation

We determined for each cell if there were significant variations in firing rate across the 16 hues by computing the coefficient of variation (the ratio of the standard deviation across hues to the mean) of the data recorded for the neuron compared to the distribution of coefficients of variation obtained by 1000 permutations of hue labels. We considered color modulation to be significant when the p-value was below $\alpha = 0.05$.

Vector sum

Color responses were also quantified by determining the vector sum of the color response. This analysis is enabled because hues are circularly distributed: we can consider the neuron's response to a hue as a vector whose direction is the hue angle, and the vector norm is the strength of the response within the response window compared to baseline. We normalized the vector norms among hues so that the total sum over hues was one. The strength of the hue preference is estimated by the direction and norm of the vector sum. Equation (1) describes the normalized vector computed for each hue; we then sum these vectors using equation (2).

$$\vec{\boldsymbol{v}}_{hue} = \frac{(FR_{hue} - \min(FR_{hues}))/(\max(FR_{hues}) - \min(FR_{hues}))}{\sum_{hue=1}^{16}[(FR_{hue} - \min(FR_{hues}))/(\max(FR_{hues}) - \min(FR_{hues}))]} * \begin{bmatrix} \cos\theta_{hue} \\ \sin\theta_{hue} \end{bmatrix} \quad (1)$$

$\vec{\boldsymbol{v}} = \sum_{hue=1}^{16} \vec{\boldsymbol{v}}_{hue}$ (2)

The preferred hue direction of the cell is the angle of $\vec{\boldsymbol{v}}$**.** The strength of the hue preference is the norm of $\vec{\boldsymbol{v}}$, and can take values ranging from 0 (no hue preference) to 1. The norm of the vector sum therefore reflects the narrowness of the color tuning.

Fourier analysis

Color responses can be analyzed using Fourier analysis (Krauskopf et al., 1982; Stoughton et al., 2012) that identifies the set of sine waves (frequency, phase angle, and amplitude) that capture the shape of the color-tuning function. We extracted for each cell the normalized amplitude and phase angle of the first 8 harmonics; most of the power was captured by the first two harmonics. The first harmonic has a single peak when plotted in polar coordinates of color space (i.e. a vector pointing to one color); the second harmonic identifies an axis in these coordinates (i.e. the poles of the axis identify an opponent color pair).

Correlation between fMRI and electrophysiology

We correlated the single cell activity for each of the 16 hues, as the average firing rate above background over the 400ms corresponding to 200 ms of stimulus followed by 200ms of blank screen for all single cells of all three monkeys, to the average percent signal change to these 16 hues obtained by interpolating from the signal change to the 12 hues used in the fMRI experiment (face-patches were identified over the 2 hemispheres of M1 and M2 of the current study, details of stimuli and ROI definition can be found in Rosenthal et al., 2018).

Author contributions: The experiments were designed and supervised by BRC, the stimuli were generated by JFD, the neurophysiological data were collected and pre-processed by TG, LT, and SE, the data were analyzed by MD, the paper was written by BRC.

Acknowledgements: We thank the animal care staff at the National Eye Institute, David Leopold, Chris Baker, Arash Afraz and Rosa Lafer-Sousa for helpful discussion and Isabelle Rosenthal and Theodros Haile for help with the first stages of the experiment. This work was supported by the Intramural research program of the National Eye Institute and the National Institute of Mental Health at the National Institutes of Health.

References

Bohon KS, Hermann KL, Hansen T, Conway BR (2016) Representation of Perceptual Color Space in Macaque Posterior Inferior Temporal Cortex (the V4 Complex). eNeuro 3.

Brayanov JB, Smith MA (2010) Bayesian and "anti-Bayesian" biases in sensory integration for action and perception in the size-weight illusion. J Neurophysiol 103:1518-1531.

Campbell FW, Maffei L (1971) The tilt after-effect: a fresh look. Vision Res 11:833-840.

Changizi MA, Zhang Q, Shimojo S (2006) Bare skin, blood and the evolution of primate colour vision. Biol Lett 2:217-221.

Chauhan T, Xiao K, Yates J, Wuerger S (2015) Estimating discrimination ellipsoids for skin images. Journal of vision 15:820.

Conway BR (2009) Color vision, cones, and color-coding in the cortex. The Neuroscientist : a review journal bringing neurobiology, neurology and psychiatry 15:274-290.

Conway BR (2018) The Organization and Operation of Inferior Temporal Cortex. Annu Rev Vis Sci 4:381-402.

Conway BR, Moeller S, Tsao DY (2007) Specialized color modules in macaque extrastriate cortex. Neuron 56:560-573.
Crichton S, Pichat J, Mackiewicz M, Tian G, Hurlbert AC (2012) Skin chromaticity gamuts for illumination recovery. Society for Imaging Science and Technology, Conference on Color in Graphics, Imaging, and Vision, Amsterdam, the Netherlands.
Derrington AM, Krauskopf J, Lennie P (1984) Chromatic mechanisms in lateral geniculate nucleus of macaque. J Physiol (Lond) 357:241-265.
Dubuc C, Brent LJN, Accamando AK, Gerald MS, MacLarnon A, Semple S, Heistermann M, Engelhardt A (2009) Sexual Skin Color Contains Information About the Timing of the Fertile Phase in Free-ranging Macaca mulatta. Int J Primatol 30:777-789.
Edwards R, Xiao D, Keysers C, Foldiak P, Perrett D (2003) Color sensitivity of cells responsive to complex stimuli in the temporal cortex. J Neurophysiol 90:1245-1256.
Eskew RT, Jr. (2009) Higher order color mechanisms: a critical review. Vision research 49:2686-2704.
Gerald MS, Waitt C, Little AC (2009) Pregnancy coloration in macaques may act as a warning signal to reduce antagonism by conspecifics. Behav Processes 80:7-11.
Golz J, MacLeod DI (2002) Influence of scene statistics on colour constancy. Nature 415:637-640.
Hasantash M, Lafer-Sousa R, Afraz A, Conway BR (2019) Paradoxical impact of memory on color appearance of faces. Nat Commun 10:3010.
Hiramatsu C, Melin AD, Allen WL, Dubuc C, Higham JP (2017) Experimental evidence that primate trichromacy is well suited for detecting primate social colour signals. Proc Biol Sci 284.
Kanwisher N, McDermott J, Chun MM (1997) The fusiform face area: a module in human extrastriate cortex specialized for face perception. The Journal of neuroscience : the official journal of the Society for Neuroscience 17:4302-4311.
Kemp R, Pike G, White P, Musselman A (1996) Perception and recognition of normal and negative faces: the role of shape from shading and pigmentation cues. Perception 25:37-52.
Komatsu H (1998) Mechanisms of central color vision. Current opinion in neurobiology 8:503-508.
Komatsu H, Ideura Y (1993) Relationships between color, shape, and pattern selectivities of neurons in the inferior temporal cortex of the monkey. J Neurophysiol 70:677-694.
Krauskopf J, Williams DR, Heeley DW (1982) Cardinal directions of color space. Vision research 22:1123-1131.
Kravitz DJ, Saleem KS, Baker CI, Ungerleider LG, Mishkin M (2012) The ventral visual pathway: an expanded neural framework for the processing of object quality. Trends Cogn Sci 17:26-49.
Lafer-Sousa R, Conway BR (2013) Parallel, multi-stage processing of colors, faces and shapes in macaque inferior temporal cortex. Nature neuroscience 16:1870-1878.
Lafer-Sousa R, Conway BR, Kanwisher NG (2016) Color-Biased Regions of the Ventral Visual Pathway Lie between Face- and Place-Selective Regions in Humans, as in Macaques. The Journal of neuroscience : the official journal of the Society for Neuroscience 36:1682-1697.
Lafer-Sousa R, Liu YO, Lafer-Sousa L, Wiest MC, Conway BR (2012) Color tuning in alert macaque V1 assessed with fMRI and single-unit recording shows a bias toward daylight colors. Journal of the Optical Society of America A, Optics, image science, and vision 29:657-670.
Lefevre CE, Ewbank MP, Calder AJ, von dem Hagen E, Perrett DI (2013) It is all in the face: carotenoid skin coloration loses attractiveness outside the face. Biol Lett 9:20130633.
Leopold DA, Rhodes G (2010) A comparative view of face perception. J Comp Psychol 124:233-251.
Martin PR, Lee BB, White AJ, Solomon SG, Ruttiger L (2001) Chromatic sensitivity of ganglion cells in the peripheral primate retina. Nature 410:933-936.
Nakajima K, Minami T, Nakauchi S (2017) Interaction between facial expression and color. Sci Rep 7:41019.

Nakajima K, Minami T, Tanabe HC, Sadato N, Nakauchi S (2014) Facial color processing in the face-selective regions: an fMRI study. Hum Brain Mapp 35:4958-4964.
Nestor A, Tarr MJ (2008) Gender recognition of human faces using color. Psychol Sci 19:1242-1246.
Ohayon S, Freiwald WA, Tsao DY (2012) What makes a cell face selective? The importance of contrast. Neuron 74:567-581.
Petersdorf M, Dubuc C, Georgiev AV, Winters S, Higham JP (2017) Is male rhesus macaque facial coloration under intrasexual selection? Behav Ecol 28:1472-1481.
Ponce CR, Xiao W, Schade PF, Hartmann TS, Kreiman G, Livingstone MS (2019) Evolving Images for Visual Neurons Using a Deep Generative Network Reveals Coding Principles and Neuronal Preferences. Cell 177:999-1009 e1010.
Rosenthal I, Ratnasingam S, Haile T, Eastman S, Fuller-Deets J, Conway BR (2018) Color statistics of objects, and color tuning of object cortex in macaque monkey. J Vis 18:1.
Roy S, Jayakumar J, Martin PR, Dreher B, Saalmann YB, Hu D, Vidyasagar TR (2009) Segregation of short-wavelength-sensitive (S) cone signals in the macaque dorsal lateral geniculate nucleus. Eur J Neurosci 30:1517-1526.
Setchell JM, Wickings EJ (2005) Dominance, status signals and coloration in male mandrills (Mandrillus sphinx). Ethology 111:25-50.
Simoncelli EP, Olshausen BA (2001) Natural image statistics and neural representation. Annu Rev Neurosci 24:1193-1216.
Sinha P, Balas BJ, Ostrovsky Y, Russell R (2006) Face Recognition by Humans:Nineteen Results All Computer Vision Researchers Should Know About. Proceedings of the IEEE 94:1948-1962.
Stephen ID, Law Smith MJ, Stirrat MR, Perrett DI (2009) Facial Skin Coloration Affects Perceived Health of Human Faces. Int J Primatol 30:845-857.
Stoughton CM, Lafer-Sousa R, Gagin G, Conway BR (2012) Psychophysical chromatic mechanisms in macaque monkey. The Journal of neuroscience : the official journal of the Society for Neuroscience 32:15216-15226.
Sun H, Smithson HE, Zaidi Q, Lee BB (2006) Specificity of cone inputs to macaque retinal ganglion cells. J Neurophysiol 95:837-849.
Sweeny TD, Haroz S, Whitney D (2012) Reference repulsion in the categorical perception of biological motion. Vision Res 64:26-34.
Tailby C, Solomon SG, Dhruv NT, Lennie P (2008) Habituation reveals fundamental chromatic mechanisms in striate cortex of macaque. The Journal of neuroscience : the official journal of the Society for Neuroscience 28:1131-1139.
Tsao DY, Freiwald WA, Tootell RB, Livingstone MS (2006) A cortical region consisting entirely of face-selective cells. Science 311:670-674.
Vos JJ (1978) Colorimetric and photometric properties of a 2° fundamental observer. Color Res Appl 3:125-128.
Waitt C, Gerald MS, Little AC, Kraiselburd E (2006) Selective attention toward female secondary sexual color in male rhesus macaques. Am J Primatol 68:738-744.
Waitt C, Little AC, Wolfensohn S, Honess P, Brown AP, Buchanan-Smith HM, Perrett DI (2003) Evidence from rhesus macaques suggests that male coloration plays a role in female primate mate choice. P Roy Soc B-Biol Sci 270:S144-S146.
Webster MA, MacLeod DI (2011) Visual adaptation and face perception. Philos Trans R Soc Lond B Biol Sci 366:1702-1725.
Wei XX, Stocker AA (2015) A Bayesian observer model constrained by efficient coding can explain 'anti-Bayesian' percepts. Nat Neurosci 18:1509-1517.
Yamashita JA, Hardy JL, De Valois KK, Webster MA (2005) Stimulus selectivity of figural aftereffects for faces. J Exp Psychol Hum Percept Perform 31:420-437.

Yip AW, Sinha P (2002) Contribution of color to face recognition. Perception 31:995-1003.
Zaidi Q, Marshall J, Thoen H, Conway BR (2014) Evolution of neural computations: Mantis shrimp and human color decoding. Iperception 5:492-496.

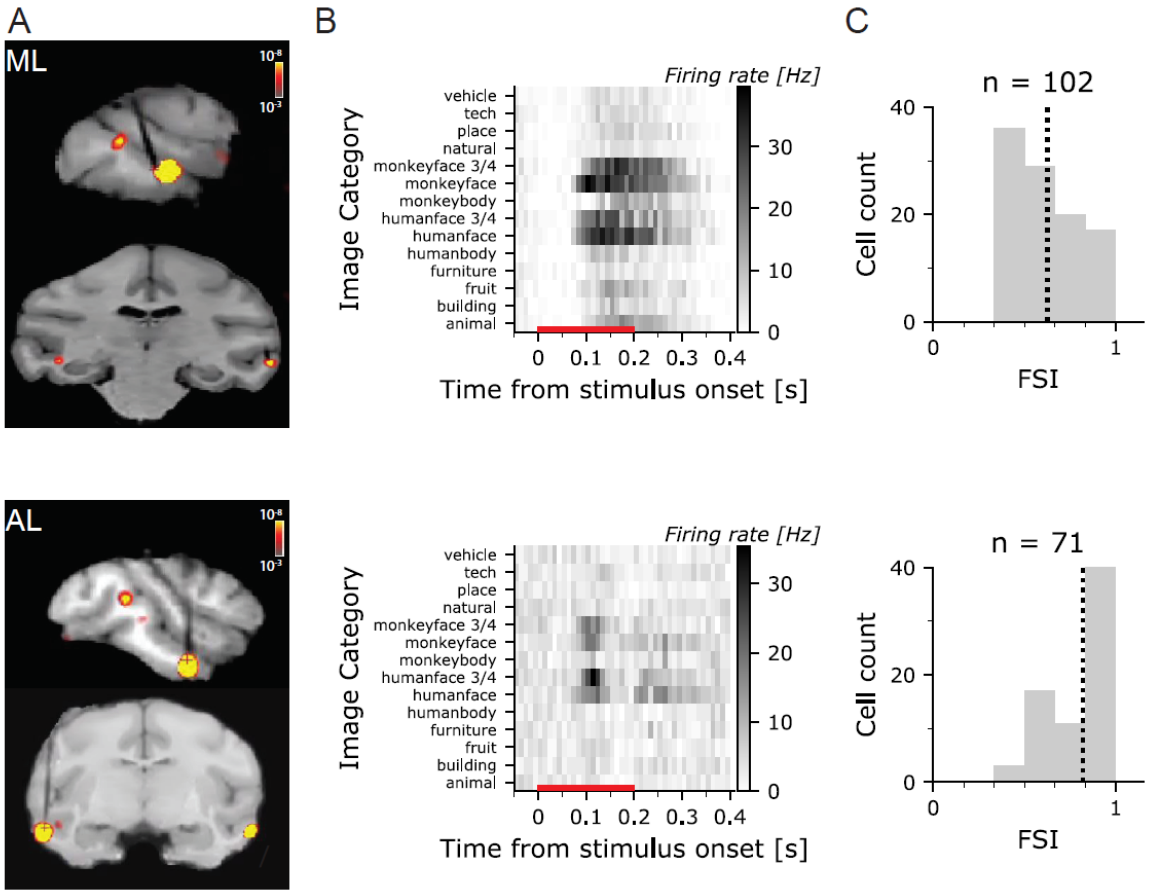

Figure 1. FMRI-guided microelectrode recording of face-selective cells in macaque inferior temporal cortex. **A.** Sagittal MR Images with recording micro-electrodes; superimposed is shown the fMRI contrast maps of faces>bodies uncover the face patches (ML-M2 top; AL-M3 bottom). Electrodes appear black in the MRI images, and target the face patches. **B**. Post-stimulus time histogram for an example cell in ML (top) and AL (bottom) showing the responses to achromatic images used to identify face cells. The red line along the x-axis shows the stimulus duration. **C.** Histogram showing the face-selectivity index (FSI) for the population of face cells in ML (top) and AL (bottom); the dashed vertical line shows the mean FSI. All cells with an FSI>=1/3 were included in the analysis.

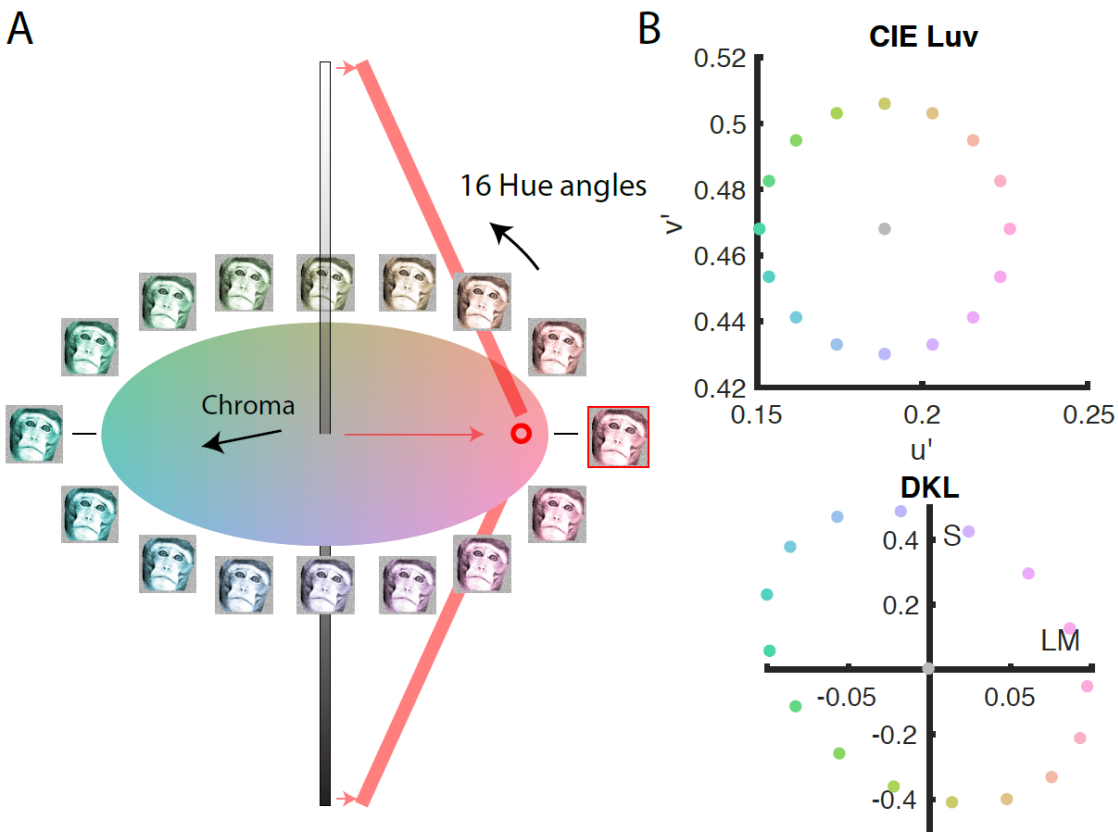

Figure 2. Stimuli used to measure the color responses of face-selective cells in macaque inferior temporal cortex. **A.** Color space illustrating the procedure for generating the colored images. Each colored image was generated by replacing the pixels in the original achromatic image with a given hue that preserved the luminance of original pixel. **B.** Sixteen colored versions were generated; the chromaticity of the most saturated pixel in each version is shown in CIELUV (u*, v*; top panel) and cone-opponent color space (DKL, bottom panel).

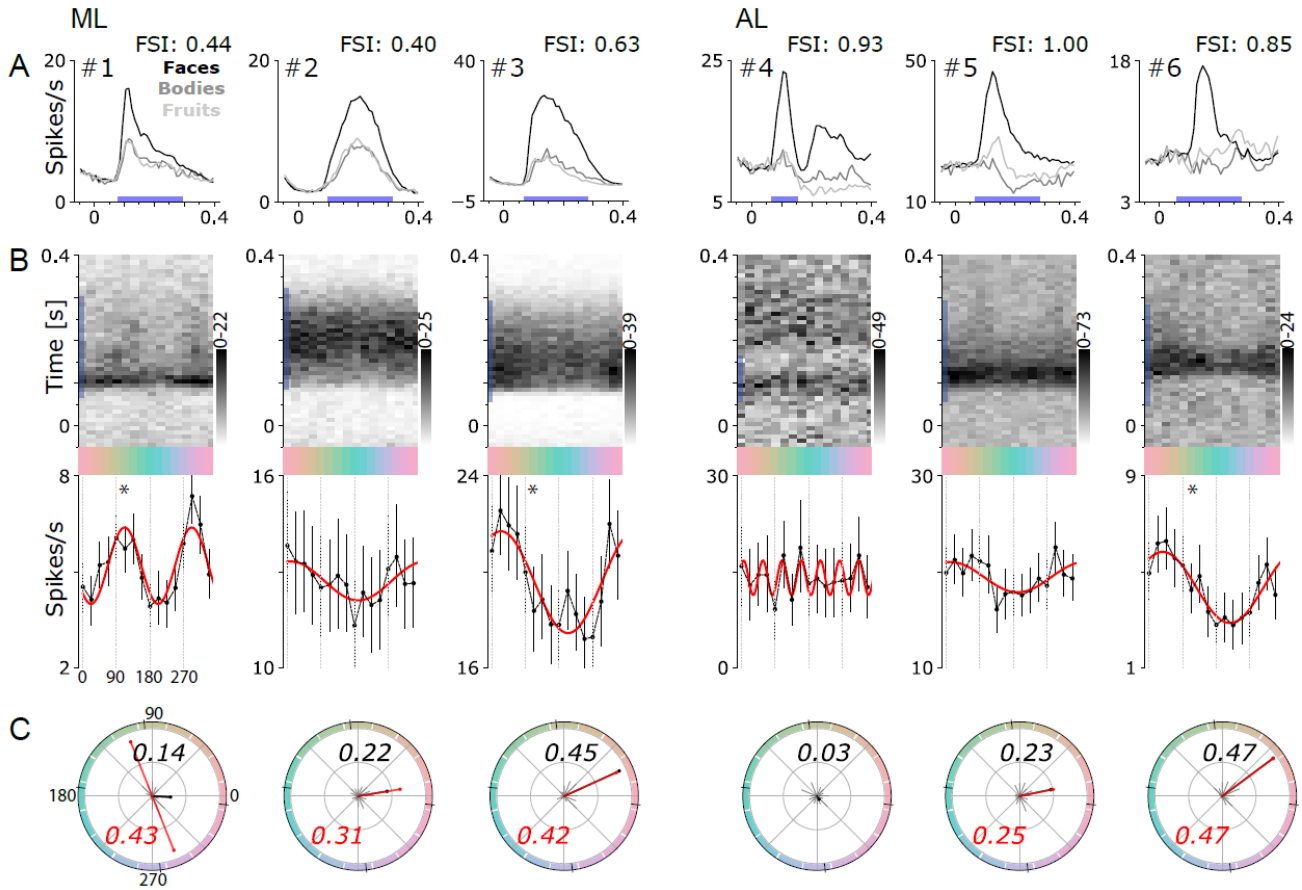

Figure 3. Responses to color of six face-selective cells in macaque inferior temporal cortex (2 cells for each monkey M1: #2, 3 – M2: #1, 5 – M3: #4, 6). **A.** Average responses to images of faces, bodies, and fruits. The time period during which the responses were quantified in subsequent analyses is shown by the blue bar along the x-axis. **B.** Post-stimulus time histogram (top panels) showing the average responses to colored images of faces; blue bar along the time axis as in panel A. Average response to face images of each color (bottom), quantified during the time period indicated by the blue bar in A and B. Error bars show 95% confidence intervals; the red line shows the best fitting sine wave. **C.** Polar plot showing normalized responses to all hues; the sum of the responses to the 16 colors is normalized to equal 1. The bold black text states the norm of the vector sum. The red line shows the normalized amplitude and phase of the best fitting sine wave for neurons whose best fit was a first or second harmonic; the red text states the value of the normalized amplitude of the best-fitting sine. The small black lines on the edges of the circle show the cardinal axes of the cone-opponent color space.

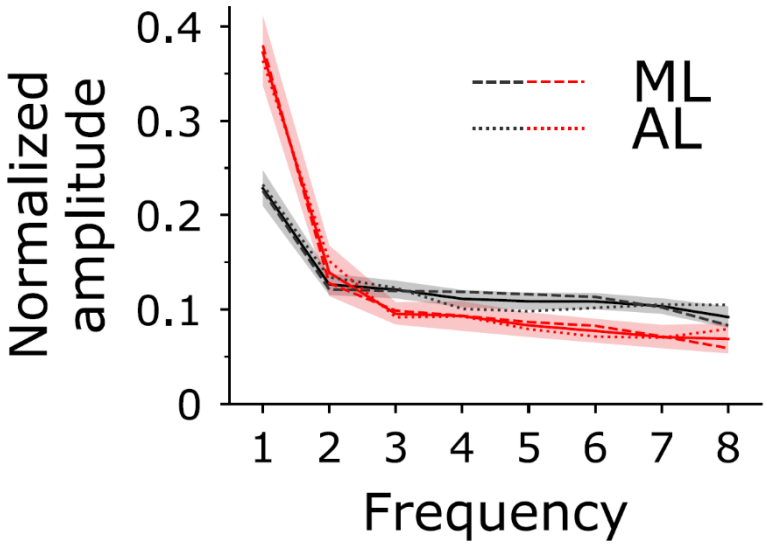

Figure 4. Power spectrum of the Fourier analysis of the color-tuning responses of face-selective neurons in macaque inferior temporal cortex. Average normalized amplitude of each harmonic component for the population (in black) and for significantly color tuned cells (in red). Surrounding shaded areas show 95% confidence intervals and dashed and dotted lines, the averages for respectively ML and AL.

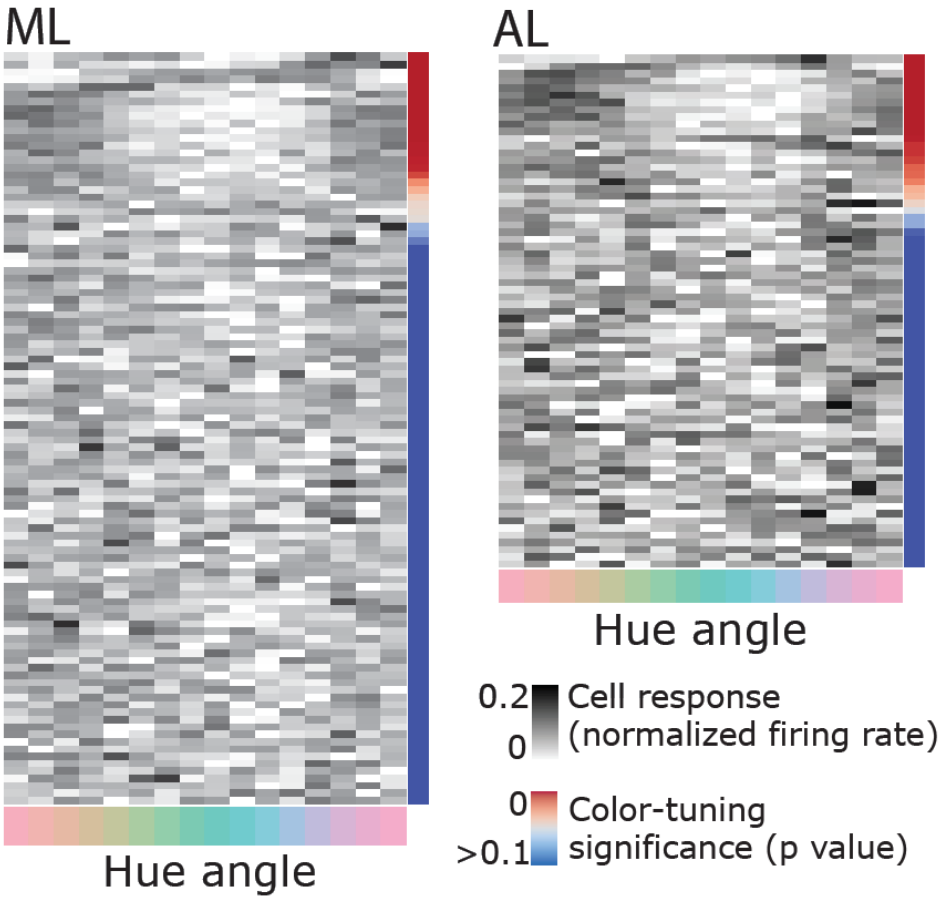

Figure 5. Responses to face images in each of 16 colors, for each cell in the ML face patch (top) and the AL face patch (bottom). Each row shows data for one cell. Cells are ordered from the top by descending color selectivity (p-value indicated by the color scale). The plot shows normalized responses: the sum of the responses to the 16 colors for each row adds up to one (darker gray indicates relatively stronger responses). A maximal preference for one hue would be indicated by black for that hue and white for all others.

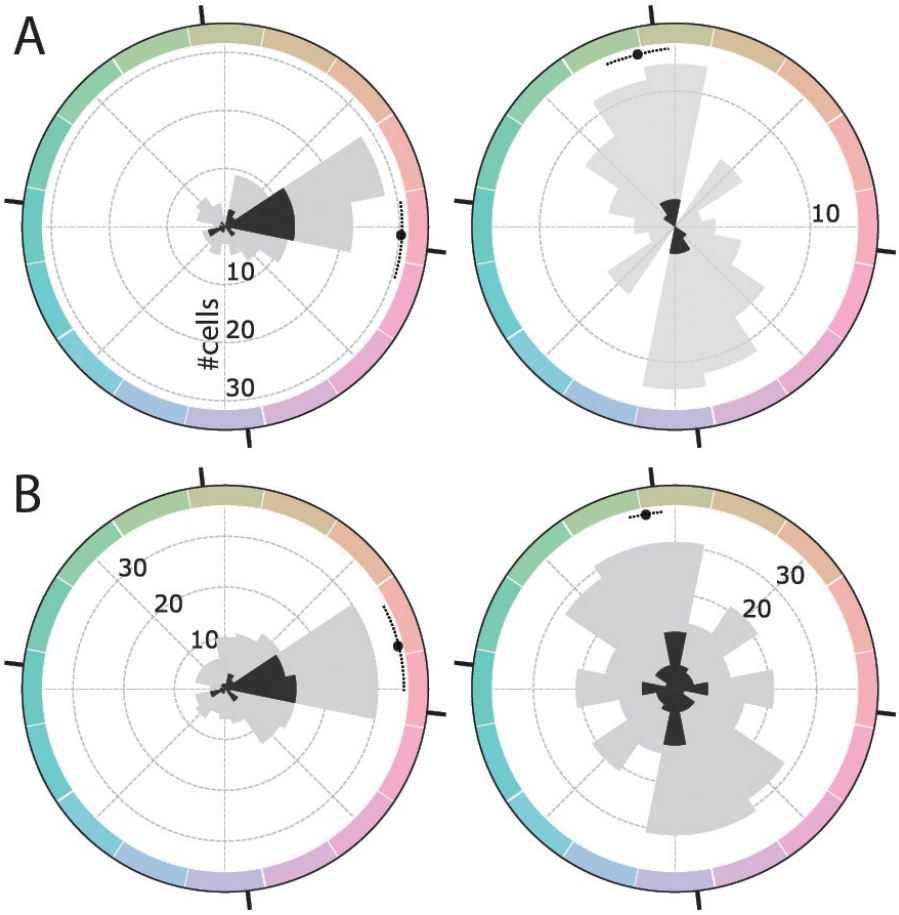

Figure 6. Fourier analysis of the color responses of face-selective cells in macaque inferior temporal cortex. **A.** Left panel shows the distribution of the phase angle for cells with higher amplitude in the first harmonic than the second harmonic (126/173 cells; Mean: -4.40 degrees CI=[-17.0,+8.5]); the right panel shows the phase angle for cells with higher amplitude in the second harmonic compared to the first harmonic (47/173 cells; Mean: +102.7 degrees CI=[+94.5,+111.1]). **B.** Distribution of the phase angle for the whole population (173 cells) for the first harmonic (left panel; mean +13.3 degrees CI=[-0.1,+27.9]) and the second harmonic (right panel; Mean: +99.6 degrees CI=[+94.2,+105.3]). The color space is CIELUV; black tick marks are provided for the cardinal axes of the cone-opponent DKL color space (these are offset from the axes of CIELUV by 6.7 degrees).

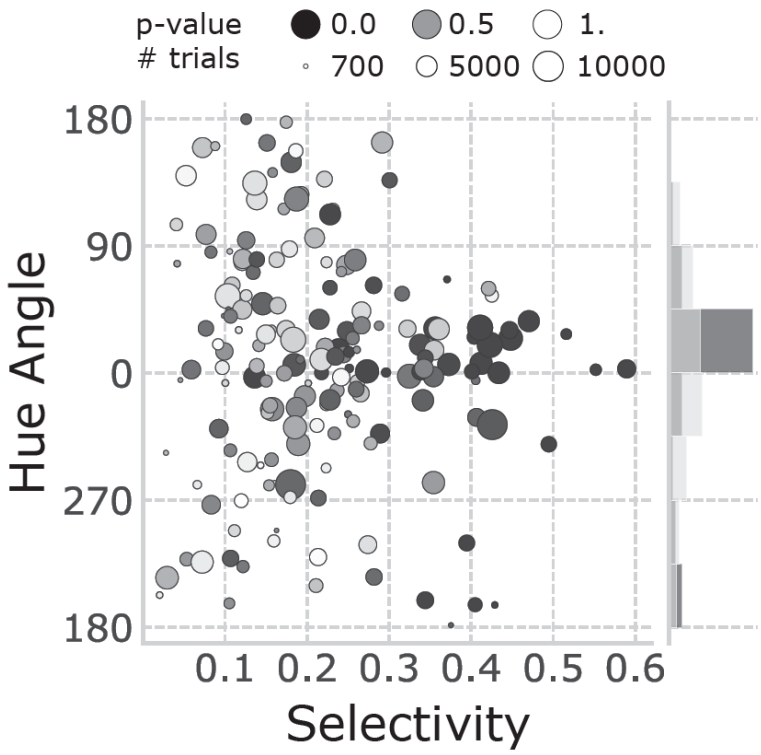

Figure 7. Quantification of the color responses of face-selective cells. Preferred hue angle (direction of the average vector) is plotted as a function of the strength of the color preference (norm of the average vector). Each face-selective cell is represented by a dot. The symbol size corresponds to the number of stimulus presentations. The gray value of the symbols reflects the significance of the color modulation (p-value). The marginal distribution shows the normalized distribution of the preferred hue for significantly (dark grey) and non-significantly (light grey) color-tuned cells.

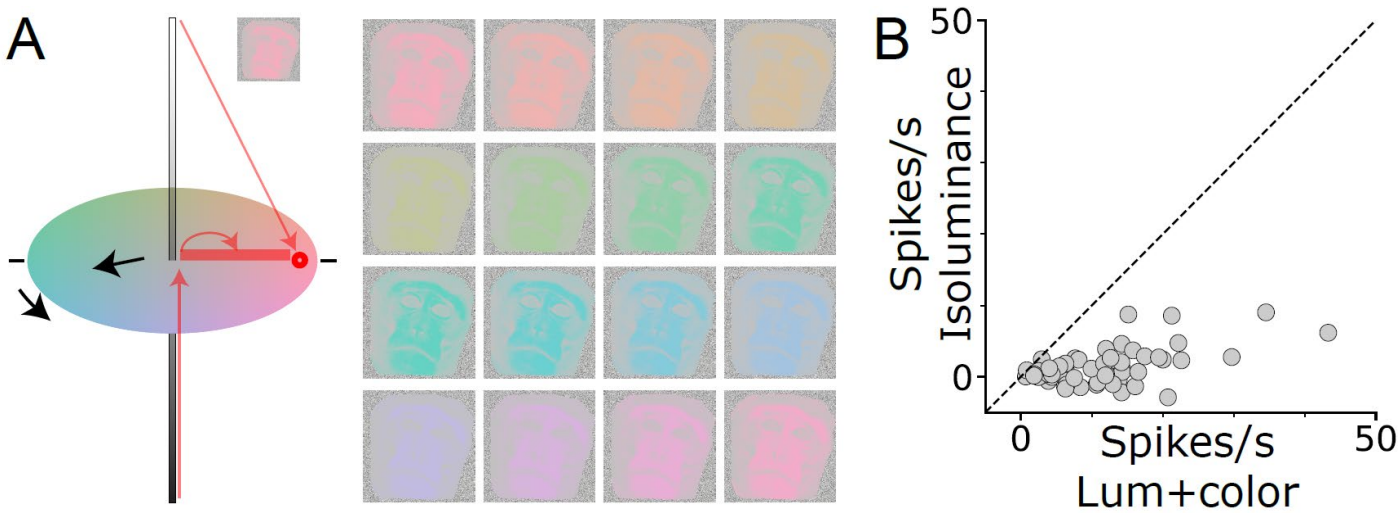

Figure 8. Response to equiluminant stimuli. **A.** Illustration of the construction of an L>M colored image. The range of gray values in the original image were replaced with colors defined by a vector along an equiluminant plane in the color space: white pixels of the original image were rendered in a saturated hue; black pixels were rendered in gray; and gray pixels were rendered in a hue of intermediate saturation. **B.** Firing rate above background of a population of face-selective neurons to equiluminant stimuli (x-axis) versus luminance-preserved colored stimuli (yaxis; N=71 cells), each dot represents one cell.

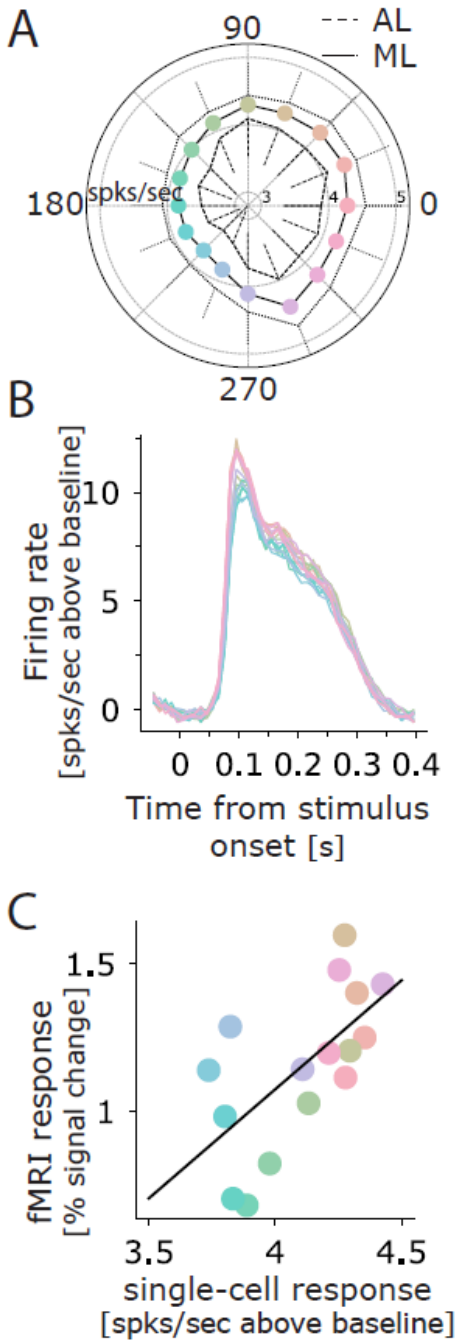

Figure 9. Comparison of color tuning measured using microelectrode recording of single cells in face patches and fMRI. **A.** Average above-background firing rate computed over a 400 ms time window that begins with the stimulus onset. The stimulus duration was 200 ms and there was a 200 ms inter-stimulus interval. **B.** Average above-background response for all face-selective cells (N=173) to face images in 16 colors (the color of the traces corresponds to the colors of the images, see Figure 2). **C.** Correlation between average response across the population of single units and fMRI color tuning assessed in the face patches of monkeys M1 and M2 (see Methods).

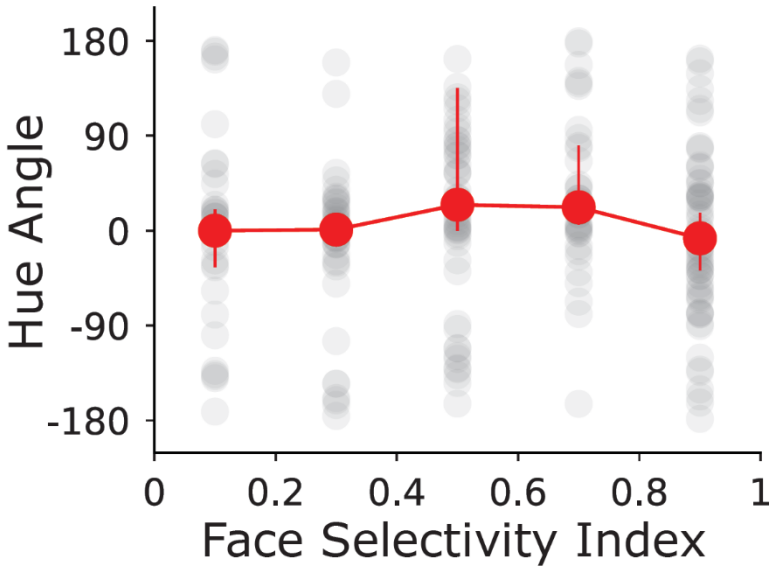

Figure 10. Median hue angles and 95% confidence intervals on the median as a function of Face Selectivity Index are represented in red. Dots represent the values in one bin of 0.2.

	M1			*M2*			*M3*			*Total*		
	#cells	latency	duration	#cells	latency	duration	#cells	latency	duration	#cells	latency	duration
ML	45	125	180	57	75	150	-	-	-	102	95	175
AL	7	135	160	15	95	130	49	75	60	71	85	110

Table 1. Number of cells, median latency and duration (in ms) of the response window used for the main analysis, by monkey and by face patch.

	CIE xyY			***CIE Luv***		***DKL***	
	x	y	Y	u'	v'	LM	S
white point	0.3009	0.3311	56.5	0.1889	0.4677	0	0
hue 0°	0.3473	0.3183	56.5	0.2268	0.4677	0.0979	0.0547
hue 22.5°	0.3581	0.3427	56.5	0.2239	0.4822	0.0935	0.2145
hue 45°	0.3607	0.3675	56.5	0.2157	0.4945	0.0760	0.3347
hue 67.5°	0.3536	0.3884	56.5	0.2034	0.5027	0.0483	0.4026
hue 90°	0.3370	0.4010	56.5	0.1889	0.5056	0.0145	0.4123
hue 112.5°	0.3137	0.4020	56.5	0.1744	0.5027	-0.0214	0.3637
hue 135°	0.2882	0.3909	56.5	0.1621	0.4945	-0.0550	0.2615
hue 157.5°	0.2659	0.3704	56.5	0.1538	0.4822	-0.0819	0.1164
hue 180°	0.2505	0.3450	56.5	0.1510	0.4677	-0.0979	-0.0547
hue 202.5°	0.2441	0.3196	56.5	0.1538	0.4532	-0.0995	-0.2282
hue 225°	0.2465	0.2980	56.5	0.1621	0.4409	-0.0852	-0.3754
hue 247.5°	0.2563	0.2826	56.5	0.1744	0.4326	-0.0562	-0.4678
hue 270°	0.2717	0.2747	56.5	0.1889	0.4298	-0.0171	-0.4851
hue 292.5°	0.2907	0.2748	56.5	0.2034	0.4326	0.0248	-0.4226
hue 315°	0.3111	0.2826	56.5	0.2157	0.4409	0.0617	-0.2933
hue 337.5°	0.3308	0.2975	56.5	0.2239	0.4532	0.0871	-0.1239

Table 2. Coordinates of the target hues and adaptation point in Cie xyY, CIE LUV and cone contrast spaces.